European Congress on Computational Methods
in Applied Sciences and Engineering (ECCOMAS 2012)
J. Eberhardsteiner et.al. (eds.)
Vienna, Austria, September 10-14, 2012

2D PHASE-FIELD ANALYSES OF DENDRITE AND AXON GROWTH OF NERVE CELL

Kazuya Nakagawa[1], Tomohiro Takaki[2], Yusuke Morita[3], and Eiji Nakamachi[3]

[1] Graduate school, Doshisha University, Japan
1-3 Tatara-Miyakodani, Kyotanabe, Kyoto, 610-0394, Japan
e-mail: dmm0024@mail4.doshisha.ac.jp

[2] Kyoto Institute of Technology, Japan
Matsugasaki, Sakyo, Kyoto, 606-8585, Japan
e-mail: takaki@kit.ac.jp

[3] Doshisha University, Japan
1-3 Tatara-Miyakodani, Kyotanabe, Kyoto, 610-0394, Japan
e-mail: enakamac@mail.doshisha.ac.jp

Keywords: Phase-field method, Nerve cell, Axon, Nerve regeneration, Numerical analyses

Abstract. *In the nerve regeneration process, the damaged part of the nerve is replaced by an artificial tube acting as the scaffold to induce dendritic and axonal growth through the artificial tube and regenerate the entire nerve network. Biotransformation and absorption of the scaffold complete the process. However, the mechanism of cell activation, axonal extension, and nerve network regeneration is not completely elucidated yet. In particular, the numerical technique to analyze the remodeling process of the nerve in the scaffold is strongly required to be established. In vivo experimental observation technology at the micro scale also remains an unresolved problem. In this study, we developed a new simulation code which employed the phase-field method to predict the two-dimensional dendritic and axonal growth processes of nerve cells on cultivation scaffolds. We curried out the phase-field analyses to make clear how the parameters of Kobayashi–Warren–Carter (KWC) model affected on the morphologic growths of dendrite and axon. Simultaneously, we observed the axonal extension process of PC-12D cells on a two-dimensional cultivation medium containing nerve growth factor (NGF). By comparing the numerical results with the observation ones of the axonal extension, we confirmed the validity of our newly developed phase-field simulation scheme.*

1 INTRODUCTION

Reconstructive surgery has been performed on nerves damaged by traffic accidents, excision of malignancies, etc. employing the direct suture or autologous transplantation methods. However, the direct suture method is limited to cases where the length of the damaged nerve tube is 5 mm or less, and there often occurs the size mismatches between the donor and recipient tissue, the neuroma formation, and the loss of functionality at the donor sites. To overcome these problems, the regeneration therapy for the damaged nerve by using a scaffold has attracted attention [1-3].

The scaffold used for the nerve regeneration has the tube structure with sufficient strength to hold the lumen; it needs to be biodegradable and absorbable so that it does not damage the surrounding tissue and regenerated nerve [4-8]. The axonal extension should complete nerve regeneration before the scaffold biodegradation and absorption [9-12]. Therefore, an analysis scheme to predict the axonal extension process under consideration of scaffold effects is needed for design of the scaffold. However, because *in vivo* observation of experiments is difficult, a simulation technology to predict the axonal extension is important to develop a scaffold for nerve regeneration. No effective numerical method has been developed so far because it is extremely difficult to predict the spontaneous extension and branching of an axon.

On the other hand, the phase-field method [13-18] has been applied in various fields of material science and engineering as a robust numerical scheme to solve the moving boundary phenomenon. In this study, we developed a new simulation code to predict the two-dimensional dendritic and axonal growth processes of nerve cells on cultivation scaffolds by using the phase-field method.

In a preliminary numerical study, we investigated the effects of two parameters of Kobayashi–Warren–Carter (KWC) model on the dendritic and axonal morphologic growths. Furthermore, we observed the axonal extension process of PC-12D cells in a two-dimensional cultivation medium to which nerve growth factor (NGF) was added. We compared the numerical results with the observation results of the axonal extension to confirm the validity of the newly developed phase-field simulation scheme.

2 CELL CULTURE AND TREATMENT

We performed a growth experiment on PC-12D cells to understand axonal extension process to develop a phase-field model. The PC-12D cells were cultured at 37°C under 5% CO_2 in air with Dulbecco's modified Eagle's medium containing 10% horse serum and 10% fetal bovine serum. The cell density was adjusted to 2.5×10^4 cells/ml. We disseminated the cell suspension on a dish and added 50 ng/ml NGF to the dish after checking the adhesion of the cells. After adding NGF, we observed the cells in the incubator that was set on the microscope stage. Figure 2.1 shows photomicrographs of the cell taken every 4 hrs. We found that four neurites were generated from a nerve cell body after certain periods from the beginning of observation; the axon grew from the neuritic tip. The nerve cell had a single axon; other neurites became dendrites. The axon extended into branches and came into contact with other dendrites extending from another nerve cell. When Sano [19] created an NGF gradient in the medium by using a micropipette, it was observed that the dendrites extended to the higher side of the concentration gradient.

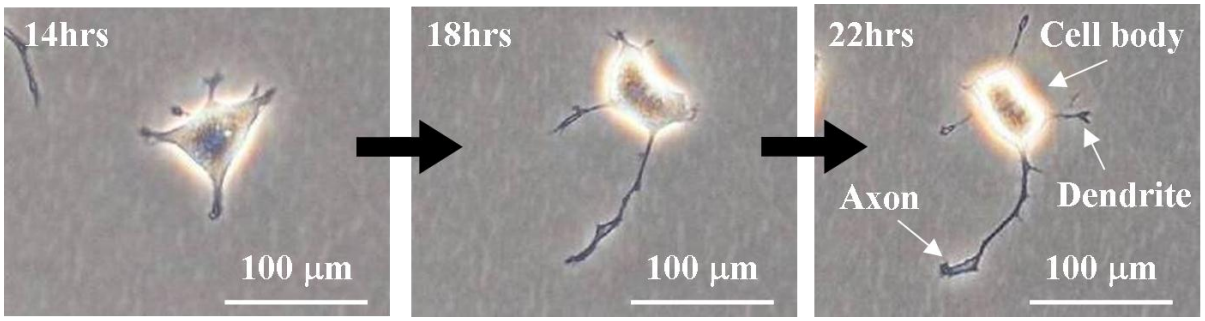

Figure 2.1: Cultivated PC-12D cells every 4 hrs after exposure to NGF

3 PHASE-FIELD MODEL

As shown in Figure 2.1, in the axonal growth experiment we first observed that several neurites sprouted from nerve cells after the providing NGF. We then observed that a thin axon grew from the neuritic tip and extended with branching.

This process of axonal extension was modeled using the phase-field method. To reproduce the branching in the growth cone, an orientation field and singular diffusion equations to express the orientation rotation are introduced. We adopted the KWC model [20-22], which was used to simulate the spherulite formation during solidification of the polymer material [23-25].

In this model, three order variables—the phase-field ϕ, orientation θ, and concentration c—are used. The phase-field ϕ takes a value of 1 in the cell and 0 in the solution (hereafter referred to as liquid); the solution surrounds the cell and includes nutritional factors such as NGF, ϕ changes smoothly at the interface region, as shown in Figure 3.1. The orientation θ was introduced to express axonal branching. The concentration c is the NGF concentration and expresses the fact that the axon grows by incorporating NGF. Following the Kim–Kim–Suzuki (KKS) model [26], the relationship of $c = \phi c_{cell} + (1-\phi)c_{liq}$ was assumed, where c_{cell} is the concentration inside the cell and c_{liq} is the concentration in the liquid. In addition, the ratio of c_{cell} and c_{liq} is set to be constant by the partition coefficient $k = c_{cell}/c_{liq}$.

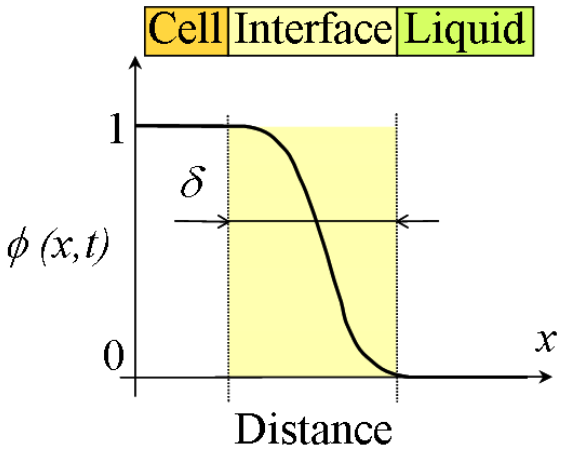

Figure 3.1: Phase-field profile at interface region

The time evolution equations for ϕ, θ, and c are derived so that the total free energy of the system decreases monotonically with time. Here we use the following free energy function:

$$F = \int_V \left(f_{chem} + f_{doub} + f_{grad} + f_{orie} \right) dV , \tag{1}$$

where f_{chem} is the free energy density of the bulk, f_{doub} is the double-well potential, f_{grad} is the gradient energy density and f_{orie} is the orientation gradient energy density. These are expressed as

$$f_{chem} = p(\phi) f^{cell} + (1 - p(\phi)) f^{liq} , \tag{2}$$

$$f_{doub} = W q(\phi), \tag{3}$$

$$f_{grad} = \frac{a^2}{2} |\nabla \phi|^2 , \tag{4}$$

$$f_{orie} = p(\phi) s |\nabla \theta|, \tag{5}$$

where $p(\phi)$ is the monotonically increasing function denoted by $p(\phi) = \phi^3 (10 - 15\phi + 6\phi^2)$ and $q(\phi)$. is the double-well function denoted by $q(\phi) = \phi^2 (1-\phi)^2$. a is the gradient coefficient considering the interface anisotropy. A normal function $a(\Theta) = \bar{a}\{1 + \xi \cos(\kappa(\Theta - \theta))\}$ is used, where Θ is the angle between the x-axis and interface normal, ξ is the anisotropy strength and κ is the anisotropy mode. The coefficients $\bar{a}$, W, s, and M_ϕ can be related to the material parameters using the following equations:

$$\bar{a} = \sqrt{\frac{3\delta\gamma}{b}} , \tag{6}$$

$$W = \frac{6\gamma b}{\delta} , \tag{7}$$

$$s = \frac{a^2}{\delta} = \frac{3\gamma}{b} , \tag{8}$$

$$M_\phi = \frac{\sqrt{2W}}{6a} M , \tag{9}$$

where δ is the interface thickness, γ is the interface energy, and $b = 2\tanh^{-1}(1 - 2\lambda)$ is a constant related to the interface thickness, λ is the phase-field value for defining the interface region; $\lambda = 0.1$ was used here. f^{cell} is the energy density of the bulk inside the cell, and f^{liq} is the energy density of the bulk in the liquid. The following relationship was assumed for f^{cell} and f^{sca}:

$$\frac{\partial f^{cell}(c_{cell})}{\partial c_{cell}} = \frac{\partial f^{liq}(c_{liq})}{\partial c_{liq}} . \tag{10}$$

The evolution equations of the phase-field ϕ, orientation θ, and concentration c are derived as

$$\frac{\partial \phi}{\partial t} = M_\phi \left[\nabla \cdot (a^2 \nabla \phi) - \frac{\partial}{\partial x}\left(a \frac{\partial a}{\partial \theta} \frac{\partial \phi}{\partial y} \right) + \frac{\partial}{\partial y}\left(a \frac{\partial a}{\partial \theta} \frac{\partial \phi}{\partial x} \right) - \Delta f \frac{dp(\phi)}{d\phi} - W \frac{dq(\phi)}{d\phi} \right], \tag{11}$$

$$\frac{\partial \theta}{\partial t} = M_\theta \nabla \cdot \left[p(\phi) s \frac{\nabla \theta}{|\nabla \theta|} \right], \tag{12}$$

$$\frac{\partial c}{\partial t} = \nabla \cdot D \left[\nabla c + \frac{(1-k)c}{1-\phi+k\phi} \nabla \phi \right], \tag{13}$$

where M_ϕ is the phase-field mobility to determine the extension rate, M_θ is the orientation mobility to determine the frequency of axonal branching in the growth cone, and D is the diffusion coefficient of NGF. To maintain the thin axon morphology, the diffusion coefficient in the cell D_{cell} was set to be much larger than that in liquid D_{liq}. The diffusion coefficient is varied smoothly within the interface using the following equation:

$$D = D_{cell} + (D_{liq} - D_{cell}) \frac{1-\phi}{1-\phi+k\phi}. \tag{14}$$

In Eq. (11), Δf is the driving force and is expressed as

$$\Delta f = f^{liq}(c_{liq}) - f^{cell}(c_{cell}) - \frac{\partial f^{liq}(c_{liq})}{\partial c_{liq}} (c_{liq} - c_{cell}). \tag{15}$$

However, we used the following relation for simplicity:

$$\Delta f = S \Delta T, \tag{16}$$

where S is the transformation entropy and ΔT is the change in temperature due to supercooling.

4 NUMERICAL SIMULATIONS

We carried out numerical simulations using the phase-field model derived in the previous section. First, we evaluated the effects of the initial orientation distribution and orientation mobility on the axonal extension morphology and determined the initial conditions and parameters. Finally, we performed axonal extension simulations and validated the model by comparing the results to results obtained from experimental observations.

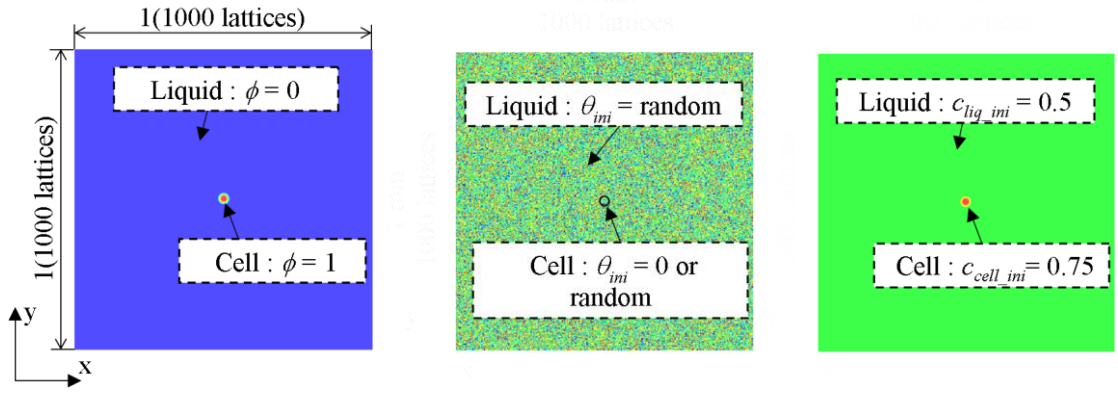

(a) (b) (c)

Figure 4.1: Simulation model and initial conditions for (a) ϕ, (b) θ, and (c) c in axonal growth simulations

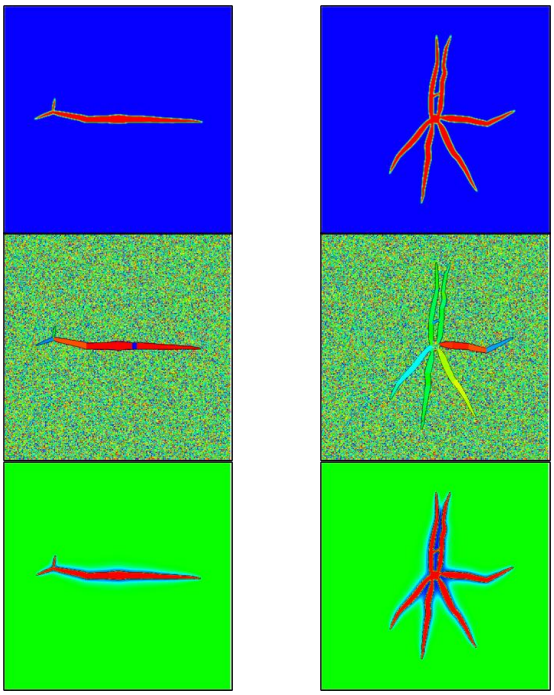

(a) $\theta_{ini} = 0$ (b) θ_{ini} = random

Figure 4.2: Effects of initial orientation on axonal growth morphology (100000 step)

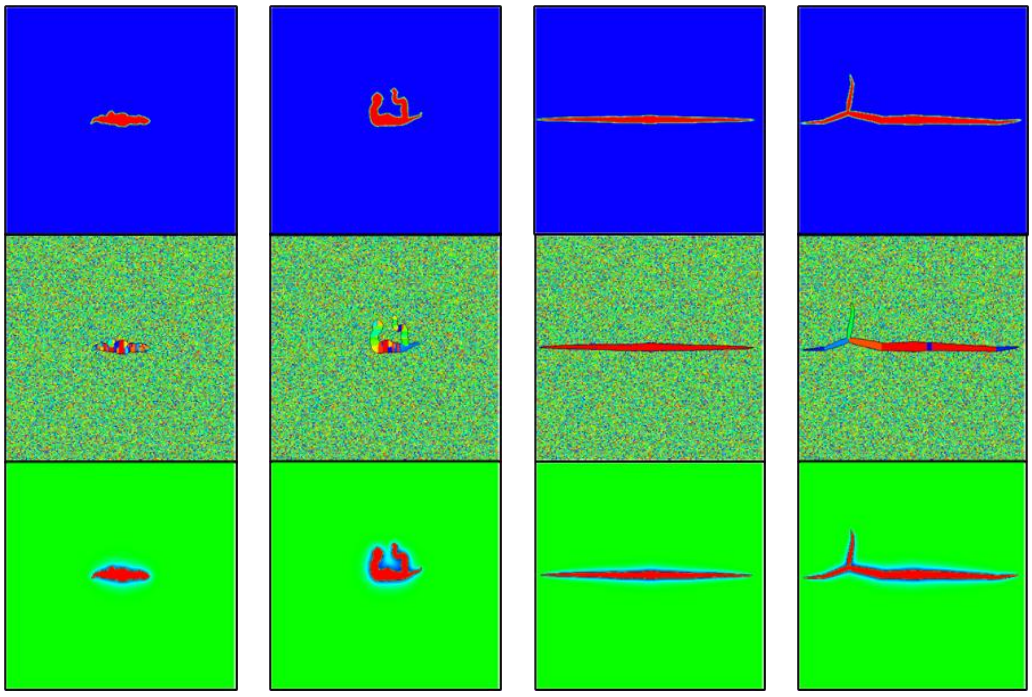

(a) $M_\theta / M_\phi = 0.05$ (b) $M_\theta / M_\phi = 0.1$ (c) $M_\theta / M_\phi = 0.5$ (d) $M_\theta / M_\phi = 1.0$

Figure 4.3: Effects of M_θ / M_ϕ on axon growth

4.1 Analysis conditions

Figure 4.1 shows our analysis model and the initial conditions in the phase-field simulation. The non-dimensional area of 1 × 1 was divided into the 1000 × 1000 finite difference grids. Thus, the grid size was $\Delta x = 0.001$. A circular cell body with a radius of $15\Delta x$ was placed in the center of the area. The initial orientation of the liquid was defined as the random value ($0 \leq \theta_{ini} \leq 1$). The initial concentrations were set to $c_{cell\_ini} = 0.75$ in the cell and $c_{liq\_ini} = 0.5$ in the liquid. The boundary condition was set to the zero Neumann boundary condition at all boundaries. The following parameters were employed: $\delta = 6\Delta x$, $\gamma = 1$, $D_{cell} = 10$, $D_{liq} = 1$, $k = 0.5$, $\kappa = 2$, $\xi = 0.5$, $M = 10$, $\Delta t = 4.0 \times 10^{-3}$. These parameters were assumed to express the nerve cell morphology.

4.2 Effects of initial orientation

We studied the effects of the orientation distribution inside the initial cell on the axonal morphologic growth. Figure 4.2 shows the calculated morphologies at step 100000 using $M_\theta / M_\phi = 0.5$. The top, middle, and bottom row figures show distribution of the phase-field variable ϕ, the orientation variable θ, and the concentration c.

In the top row of the figure, the red region ($\phi = 1$) indicates the cell morphology. The orientation has periodicity in $0 \leq \theta \leq 1$, and $\theta = 0$ and $\theta = 1$ are identical. Thus, in the middle row of the figure the red ($\theta = 1$) and blue ($\theta = 0$) regions indicate the same orientation. The bottom row of the figure shows the NGF concentration in the liquid is homogeneously. Figure 4.2 (a) is the result for a constant initial orientation $\theta_{ini} = 0$, and Figure 4.2 (b) is that for a random initial orientation in the cell.

As shown in Figure 4.2 (a), the axon grew while almost maintaining the orientation of the cell, although branching at the left tip was observed. On the other hand, Figure 4.2 (b) with an initial random orientation in the cell indicates that the neurites extended in various directions. As shown in Figure 2.1, because the cultivated nerve cell extended its neurites in various directions, the actual nerve extension can be expressed by setting the initial orientation inside the cell to a random orientation.

4.3 Effects of the orientation mobility

We investigated the effects of the ratio M_θ / M_ϕ on the morphology of axon in the phase-field simulation results. The phase-field simulations were carried out at $M_\theta / M_\phi = 0.05$, 0.1, 0.5, and 1.0 under the condition of the constant $M_\phi = 0.5$, and the initial orientation in the cell was set to a constant $\theta_{ini} = 0$. The calculated morphologies at 100000 step are shown in Figure 4.3. For small M_θ / M_ϕ, the rotation rate of the orientation at the axonal tip was slow compared with the growth rate of the axonal tip. Therefore, the growth directions of the axonal tip tended to change because the orientation of the liquid was easily incorporated with the axonal tip. On the other hand, for large M_θ / M_ϕ, the rotation rate of the orientation at the axonal tip was rapid compared with the growth rate of the axonal tip. Therefore, the growth direction remained constant because the orientation of the liquid was difficult to incorporate into the axon. From these results, we concluded that the axonal branch can be reproduced by selecting the ratio of M_θ / M_ϕ appropriately. Among the four M_θ / M_ϕ values used in the present simulations, $M_\theta / M_\phi = 0.5$ appeared to be the best value for express axonal branching.

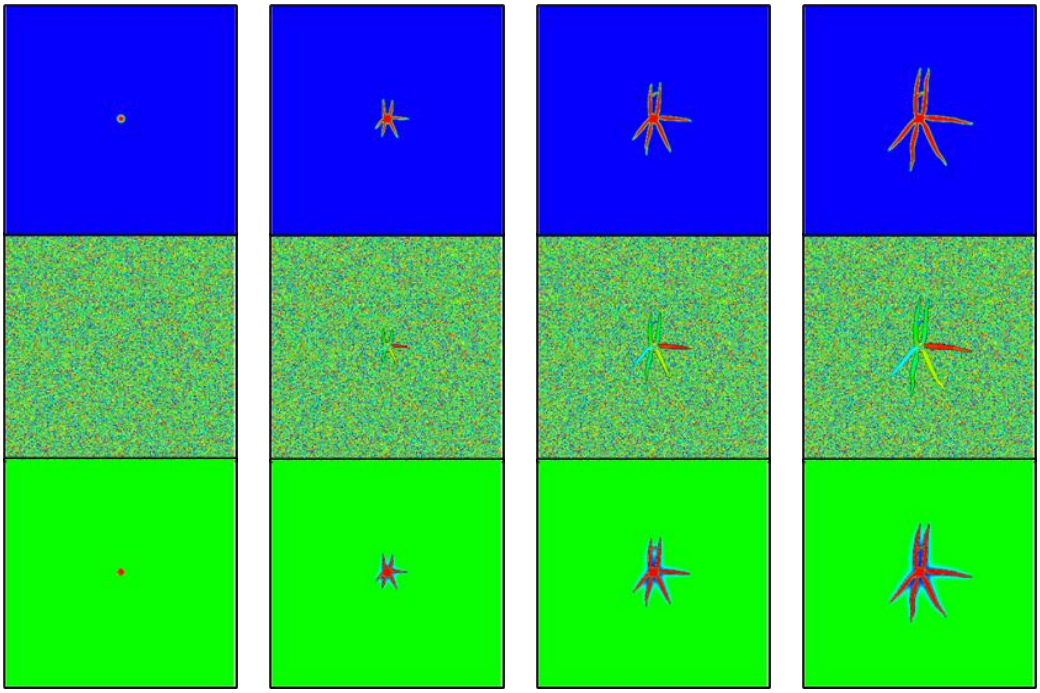

(a) initial (b) 20000 step (c) 40000 step (d) 60000 step

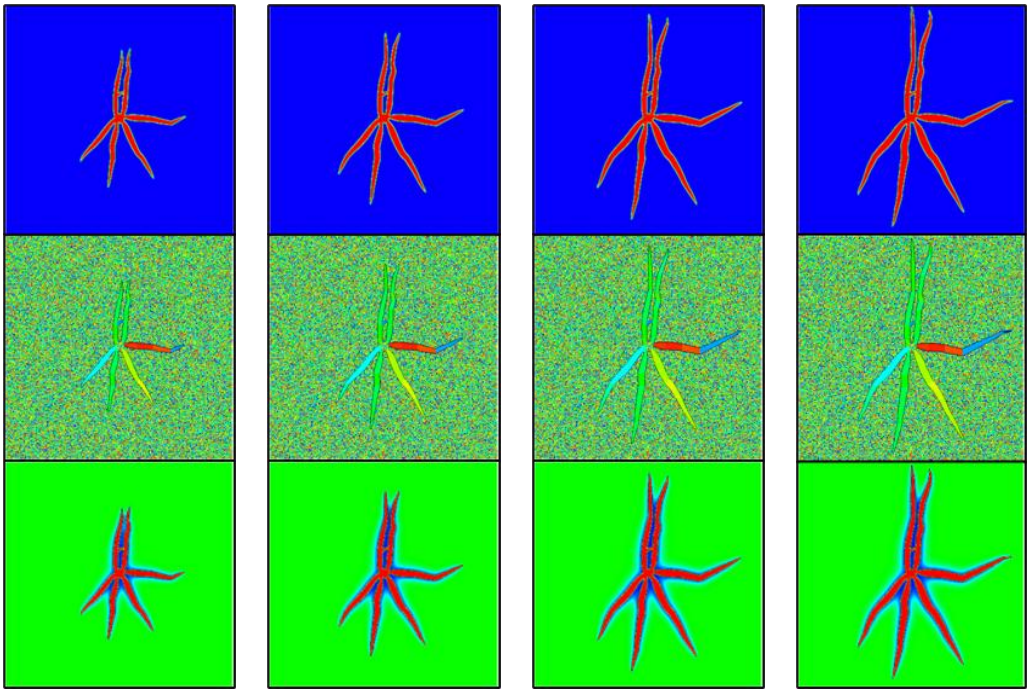

(e) 80000 step (f) 100000 step (g) 120000 step (h) 130260 step

Figure 4.4: Time evolution of axonal growth simulations

4.4 Phase-field analyses of dendritic and axonal growth of nerve cell

The preliminary computations presented in sections 4.2 and 4.3 indicated that the random initial orientation in the cell and appropriate selection of M_θ / M_ϕ resulted in realistic dendritic and axonal growth morphology. By considering these preliminary results, we simulated the

axonal extension process. The validity of the developed model was confirmed by comparing its results to the results of the experimental observations. We employ $M_\theta / M_\phi = 0.5$.

Figure 4.4 shows the results for the phase-field ϕ in the top row, orientation θ in the middle row, and concentration c in the bottom row at every 20000 steps. Figure 4.4 (a) shows the initial condition. We set the orientation in the cell placed in the center of the area to be random. As shown in Figure 4.4 (b), at 20000 step, we found evidence that six neurites started to extend. In Figure 4.4 (c), which shows further cell growth at 40000 step, an axonal branch sprouted from one out of the six neurites. However, the branch hit a neurite next to the branch, and the branch stopped extending. In Figures 4.4 (e), (f), (g), and (h) after 80000 step, changes were observed in the dendritic growth direction, by incorporating the orientation of the liquid into the cell. Furthermore, we could express the morphology of the thin dendrites by controlling the concentration field on the interface. However, when comparing our results with the observation results, we could not express the preferential growth of one dendrite that resulted in the axon.

5 CONCLUSIONS

- We developed a numerical model by applying the KWC phase-field model to predict the two-dimensional dendritic and axonal growth processes on the cultivation scaffolds.
- We succeeded to predict the dendritic extension in various directions as observed for the initial growth of the nerve cell by setting the initial orientation inside the cell to a random orientation and selecting an appropriate M_θ / M_ϕ for the axonal branch.
- When comparing our numerical results with our experimentally observation results, we could not predict accurately the facts that there occurs only one axon growth.

REFERENCES

[1] C. A. Heath, and G. E. Rutkowski: The development of bioartificial nerve grafts for peripheral-nerve regeneration, *Trends Biotechnol*, Vol. 16 (1998), 163-168.

[2] G. R. D. Evans, et al.: Bioactive poly (L-lactic acid) conduits seeded with schwann cells for peripheral nerve regeneration, *Biomaterials*, Vol. 23 (2002), 841-848.

[3] I. V. Yannas, and B. J. Hill: Selection of biomaterials for peripheral nerve regeneration using data from the nerve chamber model, *Biomaterials*, Vol. 25 (2004), 1593-1600.

[4] T. Toba, et al.: Regeneration of canine peroneal nerve with the use of a polyglycolic acid–collagen tube filled with laminin-soaked collagen sponge: A comparative study of collagen sponge and collagen fibers as filling materials for nerve conduits, *J. Biomed. Mater. Res.*, Vol. 58 (2001), 622-630.

[5] T. Nakamura, et al.: Experimental study on the regeneration of peripheral nerve gaps through a polyglycolic acid–collagen (PGA–collagen) tube, *Brain Research*, Vol. 1027 (2004), 18-29.

[6] K. Matsumoto, et al.: Peripheral nerve regeneration across an 80-mm gap bridged by a polyglycolic acid (PGA)–collagen tube filled with laminin-coated collagen fibers: a histological and electrophysiological evaluation of regenerated nerves, *Brain Research*, Vol. 868 (2000), 315-328.

[7] T. Kiyotani, et al.: Nerve regeneration across a 25-mm gap bridged by a polyglycolic acid-collagen tube: a histological and electrophysiological evaluation of regenerated nerves, *Brain Research*, Vol. 740 (1996), 66-74.

[8] A. Hagiwara, et al.: Clinical application of PGA-tube for regeneration intrapelvic nerves during extended surgery for intrapelvic recurrent rectal cancer, *Japanese Journal of Cancer and Chemotherapy*, Vol.29 (2002), 2202 – 2204.

[9] G. R. D. Evans, et al.: In vivo evaluation of poly (L-lactic acid) porous conduits for peripheral nerve regeneration, *Biomaterials*, Vol. 20 (1999), 109-1115.

[10] J. Li, and R. Shi: Fabrication of patterned multi-walled poly-l-lactic acid conduits for nerve regeneration, *Journal of Neuroscience Methods*, Vol. 165 (2007), 257-264.

[11] A. K. Kitahara, et al.: Evaluation of collagen nerve guide in facial nerve regeneration, *The Japanese Society for Artificial Organs*, Vol. 1 (1998), 22-27.

[12] F. Langone, et al.: Peripheral nerve repair using a poly(organo)phosphazene tubular prosthesis, *Biomaterials*, Vol. 16 (1995), 347-353.

[13] J. A. Warren, et al.: Extending phase field models of solidification to polycrystalline materials, *Acta Materialia*, Vol. 51 (2003), 6035-6058.

[14] R. Kobayashi: Modeling and numerical simulations of dendritic crystal growth, *physica D*, Vol.63 (1993), 410-423.

[15] A. Karma, et al.: Quantitative phase-field modeling of dendritic growth in two and three dimensions, *Phys. Rev. E*, Vol. 57 (1998), 4323-4349.

[16] M. Ode, et al.: Phase-field model for solidification of ternary alloys, *ISIJ Int.*, Vol. 40 (2000), 870-876.

[17] Y. Natsume, et al.: Phase-field Simulation of Transient Liquid Phase Bonding Process of Ni Using Ni – P Binary Filler Metal, *Mater. Trans.*, Vol. 44 (2003), 819-823.

[18] Y. Natsume, et al.: Analysis of Growth Behavior of a Cellular and Dendritic Interface under a Constrained Growth Condition using a Phase-Field Model, *Mater. Trans.*, Vol.44 (2003), 824-828.

[19] M. Sano: A new model for the study of the cellular action of NGF, PC12D cell, *J. Kyoto Pref. Univ. Med*, Vol. 108 (1999), 667-678.

[20] R. Kobayashi, J. A. Warren, and W. C. Carter: Vector-valued phase field model for crystallizetion and grain boundary formation. *Physica D*, Vol. 119 (1998), 415-423.

[21] R. Kobayashi, J. A. Warren, and W. C. Carter: A continuum model of grain boundaries, *Physica D*, Vol.140 (2000), 141-150.

[22] J. A. Warren, R. Kobayashi, and W. C. Carter: Modeling grain boundaries using a phase-field technique, *J. Cryst. Growth*, vol.211 (2000), 18-20.

[23] L. Gránásy, T. Pusztai, T. Börzsönyi, J. A. Warren, and J. F. Douglas: A general mechanism of polycrystalline growth. *Nature materials*, Vol. 3 (2004), 645-650.

[24] L. Gránásy, T. Pusztai, and J. A. Warren: Modeling polycrystalline solidification using phase field theory. *Journal of Physics: Condensed Matter*, Vol. 16 (2004), R1205-R1235.

[25] M. Asanishi, T. Takaki, and Y. Tomita: Polymer spherulite growth simulation during crystallization by phase-field method, *Proceedings of International Conference on Advances and Trends of Engineering Materials and Their Applications*, (2007), 195-203.

[26] S. G. Kim, et al.： Phase-field model for binary alloys, *Phys. Rev. E*, Vol. 60 (1999), 7186-7197.